

# Comparison of Microsphere-Equivalent Blood Flow ( $^{15}\text{O}$ -Water PET) and Relative Perfusion ( $^{99\text{m}}\text{Tc}$ -Tetrofosmin SPECT) in Myocardium Showing Metabolism–Perfusion Mismatch

Wolfgang M. Schaefer, MD, PhD<sup>1</sup>; Bernd Nowak, MD<sup>1</sup>; Hans-Juergen Kaiser, PhD<sup>1</sup>; Karl-Christian Koch, MD<sup>2</sup>; Stephan Block, MD<sup>1</sup>; Juergen vom Dahl, MD<sup>2</sup>; and Udalrich Buell, MD<sup>1</sup>

<sup>1</sup>Department of Nuclear Medicine, University Hospital, Aachen University of Technology, Aachen, Germany; and <sup>2</sup>Department of Internal Medicine I (Cardiology), University Hospital, Aachen University of Technology, Aachen, Germany

Myocardial perfusion imaging with  $^{99\text{m}}\text{Tc}$ -tetrofosmin is based on the assumption of a linear correlation between myocardial blood flow (MBF) and tracer uptake. However, it is known that  $^{99\text{m}}\text{Tc}$ -tetrofosmin uptake is directly related to energy-dependent transport processes, such as  $\text{Na}^+/\text{H}^+$  ion channel activity, as well as cellular and mitochondrial membrane potentials. Therefore, cellular alterations that affect these energy-dependent transport processes ought to influence  $^{99\text{m}}\text{Tc}$ -tetrofosmin uptake independently of blood flow. Because metabolism ( $^{18}\text{F}$ -FDG)–perfusion ( $^{99\text{m}}\text{Tc}$ -tetrofosmin) mismatch myocardium (MPMM) reflects impaired but viable myocardium showing cellular alterations, MPMM was chosen to quantify the blood flow-independent effect of cellular alterations on  $^{99\text{m}}\text{Tc}$ -tetrofosmin uptake. Therefore, we compared microsphere-equivalent MBF (MBF<sub>micr</sub>;  $^{15}\text{O}$ -water PET) and  $^{99\text{m}}\text{Tc}$ -tetrofosmin uptake in MPMM and in “normal” myocardium. **Methods:** Forty-two patients with severe coronary artery disease, referred for myocardial viability diagnostics, were examined using  $^{18}\text{F}$ -FDG PET and  $^{99\text{m}}\text{Tc}$ -tetrofosmin perfusion SPECT. Relative  $^{18}\text{F}$ -FDG and  $^{99\text{m}}\text{Tc}$ -tetrofosmin uptake values were calculated using 18 segments per patient. Normal myocardium and MPMM myocardium were classified using a previously validated  $^{99\text{m}}\text{Tc}$ -tetrofosmin SPECT/ $^{18}\text{F}$ -FDG PET score. In addition,  $^{15}\text{O}$ -water PET was performed to assess kinetic-modeled MBF (MBF<sub>kin</sub>), the water-perfusable tissue fraction (PTF), and the resulting MBF<sub>micr</sub> (MBF<sub>kin</sub>·PTF), which is comparable to tracer uptake values.  $^{99\text{m}}\text{Tc}$ -tetrofosmin uptake and MBF<sub>micr</sub> values were calculated for all normal and MPMM segments and averaged within their respective classifications. **Results:** Mean relative  $^{99\text{m}}\text{Tc}$ -tetrofosmin uptake was  $86\% \pm 1\%$  in normal myocardium and  $56\% \pm 1\%$  in MPMM, showing a significant difference ( $P < 0.001$ ), as was expected from the classification. Contrary to these findings, mean MBF<sub>micr</sub> in MPMM myocardium was  $0.60 \pm 0.03 \text{ mL} \cdot \text{min}^{-1} \cdot \text{mL}^{-1}$ , which did not significantly differ from normal myocardium ( $0.64 \pm 0.01 \text{ mL} \cdot \text{min}^{-1} \cdot \text{mL}^{-1}$ ). All values are given as mean  $\pm$  SEM. **Conclusion:** Differences be-

tween reduced  $^{99\text{m}}\text{Tc}$ -tetrofosmin uptake and the unchanged MBF<sub>micr</sub> in MPMM myocardium suggest that the pathophysiologic basis of MPMM is not a blood flow reduction but cellular alterations that affect uptake and retention of  $^{99\text{m}}\text{Tc}$ -tetrofosmin independently of blood flow. Therefore, it seems that perfusion deficits in MPMM myocardium are greatly overestimated by  $^{99\text{m}}\text{Tc}$ -tetrofosmin and that it tends to give false-positive findings.

**Key Words:** metabolism–perfusion mismatch;  $^{99\text{m}}\text{Tc}$ -tetrofosmin;  $^{18}\text{F}$ -FDG; myocardial blood flow;  $^{15}\text{O}$ -water

*J Nucl Med* 2003; 44:33–39

**M**ycardial perfusion imaging with  $^{99\text{m}}\text{Tc}$ -methoxyisobutylisonitrile and  $^{99\text{m}}\text{Tc}$ -1,2-[bis(bis-2-ethoxyethyl)-phosphino]ethane ( $^{99\text{m}}\text{Tc}$ -tetrofosmin) is a well-established and widely used technique in the diagnosis of coronary artery disease (CAD). This technique is based on the assumption of a linear correlation between myocardial blood flow (MBF) and tracer uptake. Several animal trials have compared  $^{99\text{m}}\text{Tc}$ -methoxyisobutylisonitrile and  $^{99\text{m}}\text{Tc}$ -tetrofosmin uptake and MBF using radiolabeled microspheres. Most of these studies showed a good correlation between MBF and tracer uptake (1–3) within physiologic ranges. However, some animal trials indicated that in reperfused myocardium, after an episode of acute ischemia, at least  $^{99\text{m}}\text{Tc}$ -tetrofosmin uptake decreases more than does reperfusion flow, as determined with microspheres (4,5).  $^{99\text{m}}\text{Tc}$ -tetrofosmin is a monovalent lipophilic cation whose cellular uptake is related to the  $\text{Na}^+/\text{H}^+$  ion channel (6,7), as well as cellular and mitochondrial membrane potential (6–10). These energy-dependent processes might be affected by a reduced viability. Therefore, the correlation between MBF and  $^{99\text{m}}\text{Tc}$ -tetrofosmin uptake may be limited if different viability states are compared.

MBF estimation using dynamic PET with  $^{15}\text{O}$ -water overcomes these limitations because  $^{15}\text{O}$ -water is a freely

Received Nov. 26, 2001; revision accepted Apr. 26, 2002.

For correspondence or reprints contact: Wolfgang M. Schaefer, MD, PhD, Department of Nuclear Medicine, University Hospital, Aachen University of Technology, Pauwelsstrasse 30, 52074 Aachen, Germany.  
E-mail: wschaefe@nuk-gate.nukmed.rwth-aachen.de

diffusible flow tracer and distributes in tissue according to the Kety–Schmidt principle (11,12). Appropriate kinetic models describing the dynamic processes of  $^{15}\text{O}$ -water in the myocardium have been developed, and their accuracy and reproducibility have been validated (13–17).

Metabolism ( $^{18}\text{F}$ -FDG)-perfusion ( $^{99\text{m}}\text{Tc}$ -tetrofosmin) mismatch (MPMM) myocardium indicates impaired but viable myocardium (18–21) with cellular and mitochondrial alterations (22,23). We therefore chose MPMM myocardium to quantify the blood flow-independent effect of cellular alterations on  $^{99\text{m}}\text{Tc}$ -tetrofosmin uptake. We quantified and compared true MBF ( $^{15}\text{O}$ -water PET) and  $^{99\text{m}}\text{Tc}$ -tetrofosmin uptake in MPMM and normal myocardium.

Because the invasive microsphere technique, as a gold standard, is limited to animal trials, dynamic  $^{15}\text{O}$ -water PET was used for absolute quantification of MBF. Kinetic-modeled MBF (MBF<sub>kin</sub>) by  $^{15}\text{O}$ -water PET results in units of flow rates per mass ( $\text{mL} \cdot \text{min}^{-1} \cdot \text{g}^{-1}$ ) of water-perfusible tissue (13). Unlike the invasive microsphere technique and  $^{99\text{m}}\text{Tc}$ -tetrofosmin uptake values, this method does not account for the volume of the region of interest (ROI) involved. To get comparable results, a microsphere-equivalent MBF (MBF<sub>micr</sub>), which is the flow rate per ROI volume ( $\text{mL} \cdot \text{min}^{-1} \cdot \text{mL}^{-1}$ ), could be derived from the MBF calculation (13,15,16).

This study focused on the comparison of MBF<sub>micr</sub> and relative  $^{99\text{m}}\text{Tc}$ -tetrofosmin uptake values in both normal and MPMM myocardium and the resulting quantification of the influence of cellular alterations on  $^{99\text{m}}\text{Tc}$ -tetrofosmin uptake independent of blood flow.

## MATERIALS AND METHODS

### Patients

Forty-two consecutively admitted patients (35 men, 7 women; mean age  $\pm$  SD,  $63 \pm 11$  y; age range, 40–78 y; mean body mass index,  $26.0 \pm 3.3 \text{ kg} \cdot \text{m}^{-2}$ ) with severe CAD and scheduled for an  $^{18}\text{F}$ -FDG PET scan to assess myocardial viability were investigated. Thirty-three patients had a history of at least 1 previous myocardial infarction. Ten patients had 1-vessel, 12 patients had 2-vessel, and 20 patients had 3-vessel disease. The mean left ventricular ejection fraction of all 42 patients was reduced to  $38\% \pm 13\%$ . Diabetes mellitus was previously diagnosed in 9 patients. The mean fasting glucose level of all patients was  $6.9 \pm 2.1 \text{ mmol/L}$  (range, 4.6–17.7 mmol/L).

### Patient Preparation

All studies were performed on the same day with the patient supine. At presentation, all patients had fasted and had been taking their regular cardiac medication. Between injection of  $^{99\text{m}}\text{Tc}$ -tetrofosmin and SPECT acquisition, a meal was served to reduce biliary activity. To reduce myocardial fatty acid metabolism, 250 mg of acipimox were given to all patients approximately 2 h before administration of  $^{18}\text{F}$ -FDG (24). About 1 h before injection of  $^{18}\text{F}$ -FDG, nondiabetics received an oral glucose load of 50 g. Insulin (2–8 IU) was administered intravenously to diabetics 5–10 min before administration of  $^{18}\text{F}$ -FDG.

### $^{18}\text{F}$ -FDG PET

Static  $^{18}\text{F}$ -FDG PET scanning (ECAT EXACT 922/47; CTI, Knoxville, TN/Siemens Medical Systems, Inc., Hoffman Estates, IL) was performed 60 min after intravenous administration of  $223 \pm 57 \text{ MBq}$  of  $^{18}\text{F}$ -FDG. The acquisition time was 30 min for emission (2-dimensional mode) and 15 min for transmission ( $^{68}\text{Ge}/^{68}\text{Ga}$  rod sources). Attenuation-corrected images were reconstructed using filtered backprojection (Hann; cutoff, 0.4 Nyquist). The matrix size was  $128 \times 128$  pixels, and reconstruction zoom was 2.154. The resulting pixel size was  $2.39 \times 2.39 \times 3.38 \text{ mm}^3$ .

### $^{15}\text{O}$ -Water PET

A cyclotron (RDS 111; CTI/Siemens) was used to irradiate  $^{15}\text{N}$  with 11 MeV protons for production of  $^{15}\text{O}$ , which reacted to  $^{15}\text{O}$ -water in a water module (CTI/Siemens). Two dynamic resting  $^{15}\text{O}$ -water PET studies were performed on every patient and started with the beginning of intravenous injection of 700–1,000 MBq of  $^{15}\text{O}$ -water over 10 s followed by flushing of the line with 20 mL of saline solution over 20 s. Each dynamic study (2-dimensional mode) consisted of 26 frames ( $10 \times 6$  s and  $16 \times 15$  s), for a total scan time of 5 min. For a transmission scan ( $^{68}\text{Ge}/^{68}\text{Ga}$ ), 15 min elapsed between both dynamic studies to allow for decay of the  $^{15}\text{O}$  radioactivity. Attenuation-corrected images were reconstructed using filtered backprojection (Hann; cutoff, 0.4 Nyquist). The matrix size was  $128 \times 128$  pixels, and reconstruction zoom was 2.154. The resulting pixel size was  $2.39 \times 2.39 \times 3.38 \text{ mm}^3$ .

### SPECT

Myocardial perfusion SPECT was done about 60 min after injection of  $425 \pm 49 \text{ MBq}$  of  $^{99\text{m}}\text{Tc}$ -tetrofosmin using a dual-head gamma camera (Solus; ADAC Laboratories, Milpitas, CA) equipped with a low-energy all-purpose collimator. A validated method (25) using a triple-energy-window acquisition was used to correct the datasets for attenuation and scatter. This method was based on calculation of attenuation distribution. Acquisition was done with a  $360^\circ$  rotation ( $180^\circ$  per head) in 64 steps (128 projections) of 20 s each in 3 independent energy windows:  $140 \pm 14 \text{ keV}$  for emission,  $120 \pm 6 \text{ keV}$  for scatter detection, and  $90 \pm 11 \text{ keV}$  for backscatter detection. Datasets of window 1 and window 2 were processed to obtain a scatter-corrected dataset, which was then reconstructed using a Butterworth filter (cutoff, 0.7 Nyquist; order, 5; matrix,  $128 \times 128$ ) (set A). The dataset of window 3 was analyzed to derive the raw data for attenuation distribution. This dataset was reconstructed (filtered backprojection, ramp) and then optimized with a segmentation method to eliminate object-dependent variations (set B). The scatter-corrected dataset (A) was then corrected for attenuation by processing it with the segmented attenuation maps (B). Finally, a segmented attenuation and scatter-corrected dataset was obtained ( $128 \times 128$  matrix). Pixel size was then adapted to the pixel size of the PET data ( $2.39 \times 2.39 \times 3.38 \text{ mm}^3$ ).

### Data Analysis

**Reorientation and Overlay.**  $^{18}\text{F}$ -FDG PET and  $^{15}\text{O}$ -water PET studies were acquired primarily using ECAT 7.1 software (CTI/Siemens). Transaxial SPECT slices were imported into the ECAT 7.1 software. Next, all PET and SPECT images were reoriented in left ventricular short-axis slices of 1.2-cm thickness. For reorientation of the dynamic  $^{15}\text{O}$ -water PET studies, the reorientation axes of the respective  $^{18}\text{F}$ -FDG PET studies were transferred to the  $^{15}\text{O}$ -water PET studies and controlled for accuracy on early  $^{15}\text{O}$ -

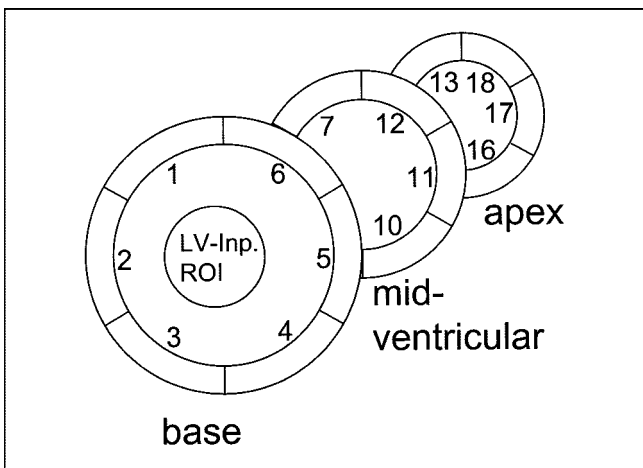


**FIGURE 1.** Definition of 18 myocardial tissue ROIs on 3 representative short-axis slices (apex, midventricular, and base). Left ventricular input (LV-Inp.) ROI is located in basal slice.

water study frames delineating the  $^{15}\text{O}$ -water–filled left ventricle chamber.

Each of 3  $^{18}\text{F}$ -FDG PET short-axis slices (apical, midventricular, basal) was divided into 6 ROIs (segments) measuring 7 mm in radial diameter (anteroseptal, septal, posteroseptal, posterolateral, lateral, and anterolateral), yielding a total of 18 segments per dataset (Fig. 1). These segments were projected to both the  $^{15}\text{O}$ -water PET images and the  $^{99\text{m}}\text{Tc}$ -tetrofosmin SPECT images.

**Quantification.** Myocardial  $^{99\text{m}}\text{Tc}$ -tetrofosmin and  $^{18}\text{F}$ -FDG PET uptake was assessed by calculating the count densities (counts per pixel) in every segment. The reference region for both  $^{99\text{m}}\text{Tc}$ -tetrofosmin and  $^{18}\text{F}$ -FDG uptake was the region with the maximum  $^{99\text{m}}\text{Tc}$ -tetrofosmin uptake. Segmental  $^{99\text{m}}\text{Tc}$ -tetrofosmin and  $^{18}\text{F}$ -FDG uptake values were then expressed as percentages of the respective reference region.

Myocardium was classified as normal if  $^{99\text{m}}\text{Tc}$ -tetrofosmin was  $>70\%$  and as MPMM if  $^{99\text{m}}\text{Tc}$ -tetrofosmin was  $\leq 70\%$ , if  $^{18}\text{F}$ -FDG

minus  $^{99\text{m}}\text{Tc}$ -tetrofosmin was  $\geq 20\%$ , and if  $^{18}\text{F}$ -FDG PET was  $>70\%$ . This classification was derived from previously reported studies on the same type of patient and using identical methods that showed that MPMM myocardium often reflects altered, dysfunctional myocardium capable of functional recovery after revascularization (18,19). Relative  $^{99\text{m}}\text{Tc}$ -tetrofosmin uptake was averaged by segment for the 6 segments and for all ROIs for both normal and MPMM myocardium.

**MBF<sub>kin</sub> and MBF<sub>micr</sub>.** MBF and water-perfusable tissue fraction (PTF) were calculated for each myocardial segment with a previously validated fitting routine based on a single-tissue-compartment model (11,12). The arterial input function was obtained from an ROI placed in the left ventricular chamber close to the base (26). MBF<sub>kin</sub> was calculated as flow rate per mass of myocardium that is capable of rapidly exchanging radiolabeled  $^{15}\text{O}$ -water ( $\text{mL} \cdot \text{min}^{-1} \cdot \text{g}^{-1}$ ). MBF<sub>kin</sub> is free of the so-called partial-volume effect (PVE) due to the PTF, which is defined as the ratio of the mass of perfusible tissue within a given ROI to the volume of that ROI ( $\text{g/mL}$ ) (13,15,16). The product of MBF<sub>kin</sub> and PTF reflects the non-PVE-corrected blood flow in this ROI volume (13,15,16) in  $\text{mL} \cdot \text{min}^{-1} \cdot \text{mL}^{-1}$  and was therefore termed the MBF<sub>micr</sub> (15).

To prove that the inversion of the PVE correction of MBF<sub>kin</sub> works well, MBF<sub>kin</sub>, PTF, MBF<sub>micr</sub>,  $^{99\text{m}}\text{Tc}$ -tetrofosmin, and  $^{18}\text{F}$ -FDG uptake values were quantified in ROIs of different sizes (Fig. 2A), all containing approximately the same myocardial mass, as described by Iida et al. (13). The dependence of the quantities on the ROI volumes is shown in Figure 2B.

MBF<sub>micr</sub> ( $\text{mL} \cdot \text{min}^{-1} \cdot \text{mL}^{-1}$ ) values were calculated for each segment, and the results of both runs were averaged. The mean MBF<sub>micr</sub> of all 6 segments (anteroseptal, septal, posteroseptal, posterolateral, lateral, and anterolateral) and of all ROIs was calculated for both normal and MPMM myocardium.

**Segmental MPMM-to-Normal Percentages.** For each of the 6 segments, both the MBF<sub>micr</sub> and the relative  $^{99\text{m}}\text{Tc}$ -tetrofosmin uptake values in MPMM myocardium were divided by the seg-

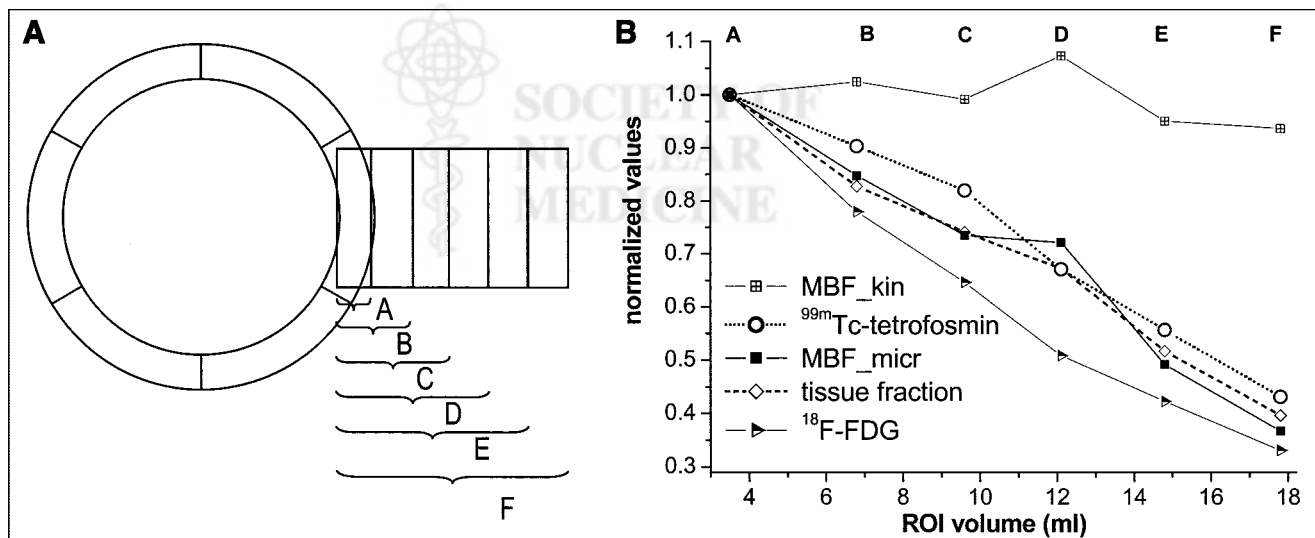


**FIGURE 2.** (A) ROIs with increased volumes but all containing approximately same myocardial mass. (B) ROI volume dependencies of MBF<sub>kin</sub>,  $^{99\text{m}}\text{Tc}$ -tetrofosmin uptake, MBF<sub>micr</sub>, tissue fraction, and  $^{18}\text{F}$ -FDG uptake. All values are expressed as ratios of respective value with A (smallest ROI).

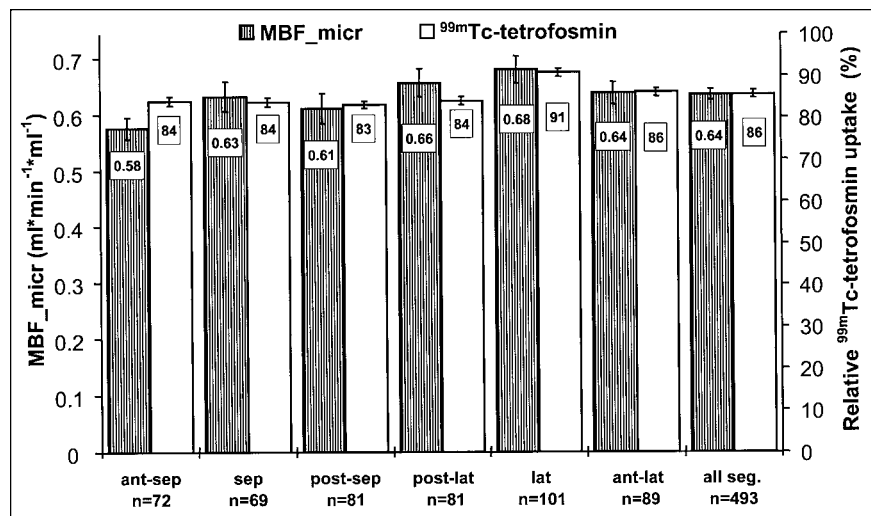


**FIGURE 3.** Mean MBF<sub>micr</sub> ( $\text{mL} \cdot \text{min}^{-1} \cdot \text{mL}^{-1}$ ) and relative  $^{99\text{m}}\text{Tc}$ -tetrofosmin uptake of investigated 6 segments and of all segments classified as normal (abscissa).  $^{99\text{m}}\text{Tc}$ -tetrofosmin uptake values are normalized to respective patient's maximum uptake region, set as 100%. Ant = anterior; lat = lateral; post = posterior; seg. = segments; sep = septal.

mental averaged corresponding values in normal myocardium, yielding the segmental MPMM-to-normal percentages.

### Statistical Analysis

All statistical analyses used SPSS 10 (SPSS Inc., Chicago, IL). Data are shown as mean  $\pm$  SEM. Differences were tested for significance using a nonparametric rank sum test (Mann–Whitney *U* test).

## RESULTS

### Comparison of MBF<sub>kin</sub>, MBF<sub>micr</sub>, $^{99\text{m}}\text{Tc}$ -Tetrofosmin, and $^{18}\text{F}$ -FDG Uptake in ROIs with Increasing Sizes

MBF<sub>kin</sub> values, assumed to be free of PVE, showed no significant changes with increasing ROI size. In contrast, all other parameters showed a concomitant, largely parallel decrease with increasing ROI size (Fig. 2B).

### MBF<sub>micr</sub> and $^{99\text{m}}\text{Tc}$ -Tetrofosmin Uptake in “Normal” Myocardium

The mean MBF<sub>micr</sub> of patients with severe CAD in myocardial segments classified as normal ( $n = 493$ ) was  $0.64 \pm 0.01 \text{ mL} \cdot \text{min}^{-1} \cdot \text{mL}^{-1}$ , and the respective mean relative  $^{99\text{m}}\text{Tc}$ -tetrofosmin uptake was  $86\% \pm 1\%$ .

The segmental distribution of the MBF<sub>micr</sub> values (Fig. 3) shows only a small variability within a range from  $0.58 \pm 0.02 \text{ mL} \cdot \text{min}^{-1} \cdot \text{mL}^{-1}$  (anteroseptal regions) to  $0.68 \pm 0.02 \text{ mL} \cdot \text{min}^{-1} \cdot \text{mL}^{-1}$  (lateral regions). Similarly, the  $^{99\text{m}}\text{Tc}$ -tetrofosmin uptake shows a small variation over the segments from  $83\% \pm 1\%$  (posteroseptal regions) to  $91\% \pm 1\%$  (lateral regions). Figure 3 shows that both MBF<sub>micr</sub> and  $^{99\text{m}}\text{Tc}$ -tetrofosmin uptake tend toward higher values in the lateral than in the septal regions.

### MBF<sub>micr</sub> and $^{99\text{m}}\text{Tc}$ -Tetrofosmin Uptake in MPMM

MBF<sub>micr</sub>, at  $0.60 \pm 0.03 \text{ mL} \cdot \text{min}^{-1} \cdot \text{mL}^{-1}$  ( $-6\%$ ), was not significantly reduced in those segments classified as MPMM ( $n = 82$ ), whereas mean relative  $^{99\text{m}}\text{Tc}$ -tetrofosmin uptake was significantly reduced to  $56\% \pm 1\%$  in MPMM

versus normal myocardium ( $-35\%$  [relative];  $P < 0.001$ ) (Fig. 4).

### Segmentwise Comparison of MPMM-to-Normal Percentages for MBF<sub>micr</sub> and $^{99\text{m}}\text{Tc}$ -Tetrofosmin Uptake

The segmental MPMM-to-normal percentage describes the relationship between MBF<sub>micr</sub> and  $^{99\text{m}}\text{Tc}$ -tetrofosmin uptake in MPMM compared with normal myocardium within the same segment. These calculations yielded values from  $81\% \pm 9\%$  (lateral regions) to  $106\% \pm 7\%$  (postero-septal regions) for MBF<sub>micr</sub> and from  $56\% \pm 6\%$  (anterolateral regions) to  $72\% \pm 3\%$  (anteroseptal regions) for  $^{99\text{m}}\text{Tc}$ -tetrofosmin uptake (Fig. 5). In all but the anteroseptal region,  $^{99\text{m}}\text{Tc}$ -tetrofosmin uptake was significantly more reduced than was MBF<sub>micr</sub>. For the septal ( $n = 24$ ), posteroseptal ( $n = 16$ ), and posterolateral regions ( $n = 17$ ), the relative differences were  $-22\%$ ,  $-37\%$ , and  $-36\%$ ,

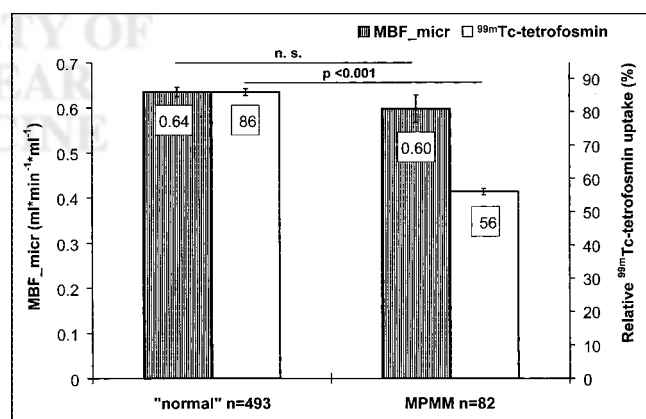


**FIGURE 4.** Mean MBF<sub>micr</sub> ( $\text{mL} \cdot \text{min}^{-1} \cdot \text{mL}^{-1}$ ) and relative  $^{99\text{m}}\text{Tc}$ -tetrofosmin uptake in normal myocardium and MPMM myocardium.  $^{99\text{m}}\text{Tc}$ -tetrofosmin uptake values are normalized to respective patient's maximum uptake region, set as 100%. n. s. = not statistically significant.

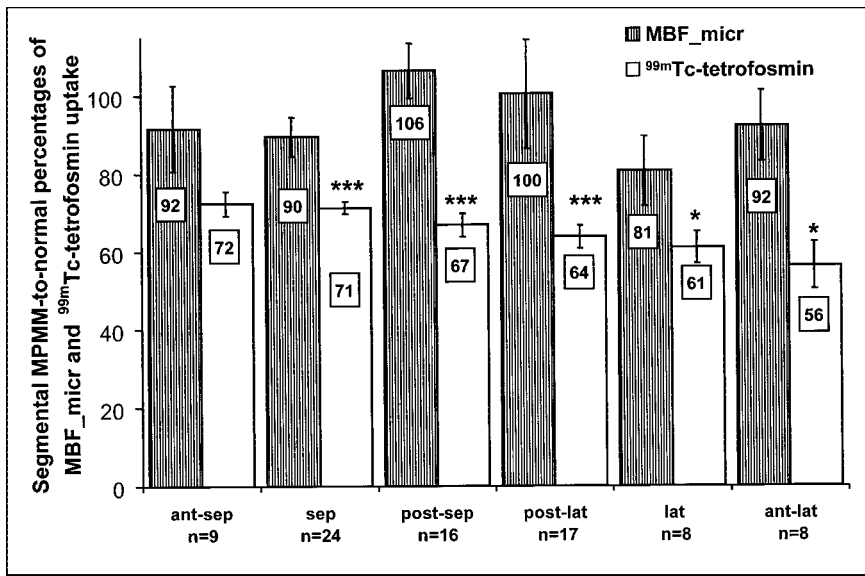


**FIGURE 5.** Segmental MPMM-to-normal percentages of mean MBF<sub>micr</sub> and relative <sup>99m</sup>Tc-tetrofosmin uptake. Mean normal values are set as 100% for each segment for either parameter. n = number of MPMM segments. \*P < 0.05. \*\*\*P < 0.005. Ant = anterior; lat = lateral; post = posterior; sep = septal.

respectively, and reached significance at  $P < 0.005$ . For the lateral ( $n = 8$ ) and anterolateral ( $n = 8$ ) regions, the relative differences were  $-25\%$  and  $-39\%$ , respectively, and reached significance at  $P < 0.05$ .

## DISCUSSION

Many studies have shown that myocardial <sup>99m</sup>Tc-tetrofosmin uptake correlates closely with blood flow (2,3), but several authors have pointed out that in animal models, <sup>99m</sup>Tc-tetrofosmin uptake is more reduced than reperfusion blood flow after acute ischemia (4,5). These findings suggest that myocardial alterations affect <sup>99m</sup>Tc-tetrofosmin uptake independently of blood flow. To overcome the limitations of a perfusion tracer whose uptake is related to energy-dependent processes ( $\text{Na}^+/\text{H}^+$  ion channel activity, cellular and mitochondrial membrane potentials (6–10)), we used <sup>15</sup>O-water PET as a reference method in assessing MBF. In this approach, relative <sup>99m</sup>Tc-tetrofosmin uptake and MBF<sub>micr</sub> were compared in normal and MPMM myocardium, and the flow-independent influence of cellular alterations on <sup>99m</sup>Tc-tetrofosmin uptake in MPMM myocardium was quantified.

The mean MBF<sub>micr</sub> ( $n = 493$ ) in normal myocardium was  $0.64 \pm 0.01 \text{ mL}\cdot\text{min}^{-1}\cdot\text{mL}^{-1}$ , which agrees with the findings of Iida et al. (15), who reported an average MBF<sub>micr</sub> of  $0.63 \text{ mL}\cdot\text{min}^{-1}\cdot\text{mL}^{-1}$  in 9 healthy volunteers. Estimation of MBF<sub>micr</sub> therefore seems to work well. In addition, the unaffected MBF<sub>micr</sub> in normal regions agrees well with the findings of Gerber et al. (27), who reported that in remote regions of dysfunctional myocardium, MBF<sub>kin</sub> was similar to that in “normal” volunteers.

As expected from our classification, <sup>99m</sup>Tc-tetrofosmin uptake in MPMM myocardium was significantly reduced, from  $86\% \pm 1\%$  (normal) to  $56\% \pm 1\%$ . Contrary to these findings, the MBF<sub>micr</sub> showed only a nonsignificant reduction, from  $0.64 \pm 0.01 \text{ mL}\cdot\text{min}^{-1}\cdot\text{mL}^{-1}$  to  $0.60 \pm 0.03$

$\text{mL}\cdot\text{min}^{-1}\cdot\text{mL}^{-1}$ . Despite the assumption of a strictly flow-proportional perfusion marker, the discrepancy between reduced <sup>99m</sup>Tc-tetrofosmin uptake and preserved MBF<sub>micr</sub> in MPMM versus normal myocardium indicates that in MPMM myocardium, processes governing <sup>99m</sup>Tc-tetrofosmin uptake or retention seem to be impaired. Contrary to these findings, <sup>15</sup>O-water diffusion along the sarcolemmal membranes was unaffected by these alterations, since otherwise the MBF<sub>micr</sub> would also have to be reduced.

Arbab et al. (6) reported that amiloride, an inhibitor of the  $\text{Na}^+/\text{H}^+$ -antiporter, reduced <sup>99m</sup>Tc-tetrofosmin uptake in cultures of rat myocardium cells by about 35%. Arbab et al. also reported that <sup>99m</sup>Tc-tetrofosmin-incubated cells released 38% of the accumulated tracer if they were treated with carbonyl cyanide m-chlorophenylhydrazone, an uncoupler of oxidative phosphorylation that depolarizes the mitochondrial membrane potential (6). Younès et al. (9) found that 2,4-dinitrophenol, another mitochondrial uncoupler, caused a 92% release of accumulated <sup>99m</sup>Tc-tetrofosmin in incubated isolated adult rat heart mitochondria. Spadafora et al. (10) reported that the cytoprotective effects of trimetazidine, which are related to the mitochondrial function and not to coronary hemodynamic changes, increased myocardial <sup>99m</sup>Tc-tetrofosmin uptake after 1 wk of administration in CAD patients. All these results indicate that <sup>99m</sup>Tc-tetrofosmin uptake and retention are related to active ion transport systems and membrane potentials as well as to mitochondrial integrity.

Comparing the unchanged MBF<sub>micr</sub> with reduced <sup>99m</sup>Tc-tetrofosmin uptake and retention suggests that the discrepancy between these 2 findings may be caused by alterations of active ion transport systems (e.g.,  $\text{Na}^+/\text{H}^+$ -antiporter), decreased membrane potentials, or ultrastructural alterations of mitochondria in MPMM versus normal myocardium. These assumptions agree well with data from Schwarz et al., who showed that ultrastructural alterations

of mitochondria, particularly reduction in size and reduction in number of cristae, are present in reversibly dysfunctional MPMM myocardium (22,23). These data also agree well with data from Ausma et al., who showed that ultrastructural alterations of mitochondria are present in reversibly dysfunctional myocardium (28).

Reduced  $^{99m}\text{Tc}$ -tetrofosmin uptake and impaired retention cannot be differentiated on the basis of these data, since acquisition was performed 60 min after injection and the resulting  $^{99m}\text{Tc}$ -tetrofosmin values are determined by uptake and retention. Studies comparing early and late  $^{99m}\text{Tc}$ -tetrofosmin SPECT are needed to differentiate between impaired uptake and retention mechanisms in these patients.

Comparing the 6% MBF\_micr flow reduction and the 35% reduction in  $^{99m}\text{Tc}$ -tetrofosmin uptake yields an approximate landmark value of about 29% for flow-independent  $^{99m}\text{Tc}$ -tetrofosmin uptake reduction between MPMM and normal myocardium. This 29% difference gives an idea of the effect of cellular alterations in MPMM myocardium on  $^{99m}\text{Tc}$ -tetrofosmin uptake independent of blood flow.

Regarding limitations of the study, the following points should be mentioned. First, the comparison of  $^{99m}\text{Tc}$ -tetrofosmin SPECT and  $^{15}\text{O}$ -water PET is a comparison of 2 different modeling techniques. The  $^{15}\text{O}$ -water model provides PVE-corrected MBF only in water-perfusable, not nonperfusible, tissue (13,15,16), whereas  $^{99m}\text{Tc}$ -tetrofosmin uptake values represent tracer accumulation within the ROI volume. However, the PTF was introduced to correct for the PVE. This PTF reflects the aspect of an ROI volume-based quantity in the  $^{15}\text{O}$ -water model. Therefore, multiplying MBF\_kin and tissue fraction reverses the PVE correction, and the resulting MBF\_micr (13,15) and  $^{99m}\text{Tc}$ -tetrofosmin uptake reflect both non-PVE-corrected ROI volume-based values and are therefore comparable. Evidence that these assumptions are correct lies in the dependency of the curves for MBF\_kin, PTF, MBF\_micr,  $^{99m}\text{Tc}$ -tetrofosmin, and  $^{18}\text{F}$ -FDG uptake on the ROI volume (Fig. 2B). The nearly parallel curves of  $^{99m}\text{Tc}$ -tetrofosmin uptake and MBF\_micr validate the mathematics underlying the PVE correction inversion, as described by Iida et al. (13), and hence prove that  $^{99m}\text{Tc}$ -tetrofosmin uptake and MBF\_micr are comparable.

Second, the comparison of  $^{99m}\text{Tc}$ -tetrofosmin SPECT and  $^{15}\text{O}$ -water PET is a comparison of different quantification (absolute vs. relative) methods. The difference between absolute and relative quantification could be eliminated by calculating the MPMM-to-normal percentages for both MBF\_micr and  $^{99m}\text{Tc}$ -tetrofosmin uptake. Therefore, comparability is given because both values are expressed as percentages.

Third, for the PET studies, attenuation was corrected by transmission measurements using  $^{68}\text{Ge}/^{68}\text{Ga}$  rod sources, whereas the SPECT studies were reconstructed using a validated attenuation and scatter correction (25) based on a triple-energy-window acquisition without a transmission scan. That the observed effects are not related to the different attenuation correction methods can be derived from the

result that the segmental MPMM-to-normal  $^{99m}\text{Tc}$ -tetrofosmin uptake percentages are significantly more reduced than the MBF\_micr percentage for all but the anteroseptal regions. Therefore, the attenuation correction applied in the SPECT studies seems to work as well as the attenuation correction by transmission scan in the PET studies for all segments.

Fourth, because the different intrinsic resolutions of the camera systems make a quantitative comparison more difficult, a flow-independent  $^{99m}\text{Tc}$ -tetrofosmin uptake reduction of about 29% can provide a landmark but not an accurate value.

## CONCLUSION

As expected from the classification, mean relative  $^{99m}\text{Tc}$ -tetrofosmin uptake is significantly reduced in MPMM myocardium, whereas mean MBF\_micr does not show a significant difference between normal and MPMM myocardium. The difference between reduced  $^{99m}\text{Tc}$ -tetrofosmin uptake and unchanged MBF\_micr can be explained by cellular alterations in MPMM myocardium, which may affect uptake and retention by impaired transport mechanisms such as active ion channel systems and membrane potentials as well as by ultrastructural mitochondrial alterations independently of blood flow. Therefore, it seems that perfusion deficits in MPMM myocardium are greatly overestimated when  $^{99m}\text{Tc}$ -tetrofosmin is used and tend to give false-positive findings.

## ACKNOWLEDGMENT

Thanks are due to Alejandro Rodón for general and language editing.

## REFERENCES

- Okada RD, Glover D, Gaffney T, Williams S. Myocardial kinetics of technetium-99m-hexamis-2-methoxy-2-methylpropyl-isotritile. *Circulation*. 1988;77:491–498.
- Sinusas AJ, Shi Q, Saltzberg MT, et al. Technetium-99m-tetrofosmin to assess myocardial blood flow: experimental validation in an intact canine model of ischemia. *J Nucl Med*. 1994;35:664–671.
- Meleca MJ, McGoron AJ, Gerson MC, et al. Flow versus uptake comparisons of thallium-201 with technetium-99m perfusion tracers in a canine model of myocardial ischemia. *J Nucl Med*. 1997;38:1847–1856.
- Glover DK, Ruiz M, Koplan BA, Watson DD, Beller GA.  $^{99m}\text{Tc}$ -tetrofosmin assessment of myocardial perfusion and viability in canine models of coronary occlusion and reperfusion. *J Nucl Med*. 1999;40:142–149.
- Takahashi N, Dahlberg ST, Gilmore MP, Leppo JA. Effects of acute ischemia and reperfusion on the myocardial kinetics of technetium 99m-labeled tetrofosmin and thallium-201. *J Nucl Cardiol*. 1997;4:524–531.
- Arbab AS, Koizumi K, Toyama K, Arai T, Araki T. Technetium-99m-tetrofosmin, technetium-99m-MIBI and thallium-201 uptake in rat myocardial cells. *J Nucl Med*. 1998;39:266–271.
- Arbab AS, Koizumi K, Toyama K, Arai T, Araki T. Ion transport systems in the uptake of 99Tcm-tetrofosmin, 99Tcm-MIBI and  $^{201}\text{Tl}$  in a tumour cell line. *Nucl Med Commun*. 1997;18:235–240.
- Platts EA, North TL, Pickett RD, Kelly JD. Mechanism of uptake of technetium-tetrofosmin. I: Uptake into isolated adult rat ventricular myocytes and subcellular localization. *J Nucl Cardiol*. 1995;2:317–326.
- Younès A, Songadele JA, Maublant J, Platts E, Pickett R, Veyre A. Mechanism of uptake of technetium-tetrofosmin. II: Uptake into isolated adult rat heart mitochondria. *J Nucl Cardiol*. 1995;2:327–333.
- Spadafora M, Cuocolo A, Golia R, et al. Effect of trimetazidine on 99Tcm-

- tetrofosmin uptake in patients with coronary artery disease. *Nucl Med Commun.* 2000;21:49–54.
11. Kety SS. Theory of blood tissue exchange and its application to measurement of blood flow. *Methods Med Res.* 1960;8:223–227.
  12. Kety SS. Measurement of local blood flow by the exchange of an inert, diffusible substance. *Methods Med Res.* 1960;8:228–236.
  13. Iida H, Kanno I, Takahashi A, et al. Measurement of absolute myocardial blood flow with  $H_2^{15}O$  and dynamic positron-emission tomography: strategy for quantification in relation to the partial-volume effect [published correction appears in *Circulation*. 1988;78:1078]. *Circulation*. 1988;78:104–115.
  14. Bol A, Melin JA, Vanoverschelde JL, et al. Direct comparison of [ $^{13}N$ ]ammonia and [ $^{15}O$ ]water estimates of perfusion with quantification of regional myocardial blood flow by microspheres. *Circulation*. 1993;87:512–525.
  15. Iida H, Rhodes CG, de Silva R, et al. Myocardial tissue fraction: correction for partial volume effects and measure of tissue viability. *J Nucl Med.* 1991;32: 2169–2175.
  16. Iida H, Tamura Y, Kitamura K, Bloomfield PM, Eberl S, Ono Y. Histochemical correlates of ( $^{15}O$ -water-perfused tissue fraction in experimental canine studies of old myocardial infarction. *J Nucl Med.* 2000;41:1737–1745.
  17. Iida H, Yokoyama I, Agostini D, et al. Quantitative assessment of regional myocardial blood flow using oxygen-15-labelled water and positron emission tomography: a multicentre evaluation in Japan. *Eur J Nucl Med.* 2000;27:192–201.
  18. vom Dahl J, Altehoefer C, Sheehan FH, et al. Recovery of regional left ventricular dysfunction after coronary revascularization: impact of myocardial viability assessed by nuclear imaging and vessel patency at follow-up angiography. *J Am Coll Cardiol.* 1996;28:948–958.
  19. vom Dahl J, Altehoefer C, Sheehan FH, et al. Effect of myocardial viability assessed by technetium-99m-sestamibi SPECT and fluorine-18-FDG PET on clinical outcome in coronary artery disease. *J Nucl Med.* 1997;38:742–748.
  20. Zhang X, Liu XJ, Wu Q, et al. Clinical outcome of patients with previous myocardial infarction and left ventricular dysfunction assessed with myocardial ( $^{99m}$ Tc-MIBI SPECT and ( $^{18}F$ -FDG PET. *J Nucl Med.* 2001;42:1166–1173.
  21. Margonato A, Chierchia SL, Xuereb RG, et al. Specificity and sensitivity of exercise-induced ST segment elevation for detection of residual viability: comparison with fluorodeoxyglucose and positron emission tomography. *J Am Coll Cardiol.* 1995;25:1032–1038.
  22. Schwarz ER, Schaper J, vom Dahl J, et al. Myocyte degeneration and cell death in hibernating human myocardium. *J Am Coll Cardiol.* 1996;27:1577–1585.
  23. Schwarz ER, Schoendube FA, Kostin S, et al. Prolonged myocardial hibernation exacerbates cardiomyocyte degeneration and impairs recovery of function after revascularization. *J Am Coll Cardiol.* 1998;31:1018–1026.
  24. Knutti MJ, Yki-Jarvinen H, Voipio-Pulkki LM, et al. Enhancement of myocardial [ $^{18}F$ ]fluorodeoxyglucose uptake by a nicotinic acid derivative. *J Nucl Med.* 1994;35:989–998.
  25. Kupferschlaeger J, Mueller B, Schulz G, et al. A method for combined scatter and attenuation correction without transmission measurement for myocardial SPECT with  $^{99m}$ Tc binding [in German]. *Nuklearmedizin.* 1997;36:56–64.
  26. Iida H, Rhodes CG, de Silva R, et al. Use of the left ventricular time-activity curve as a noninvasive input function in dynamic oxygen-15-water positron emission tomography. *J Nucl Med.* 1992;33:1669–1677.
  27. Gerber BL, Vanoverschelde JL, Bol A, et al. Myocardial blood flow, glucose uptake, and recruitment of inotropic reserve in chronic left ventricular ischemic dysfunction. Implications for the pathophysiology of chronic myocardial hibernation. *Circulation*. 1996;94:651–659.
  28. Ausma J, Thone F, Dispersyn GD, et al. Dedifferentiated cardiomyocytes from chronic hibernating myocardium are ischemia-tolerant. *Mol Cell Biochem.* 1998; 186:159–168.

